Physica D 284 (2014) 53–61

Contents lists available at ScienceDirect

Physica D

journal homepage: www.elsevier.com/locate/physd

Transient behavior of collapsing ring solutions in the critical nonlinear Schrödinger equation

Jordan Allen-Flowers [a,*], Karl B. Glasner [b]

[a] Program in Applied Mathematics, University of Arizona, Tucson, AZ, 85721, USA
[b] Department of Mathematics, University of Arizona, Tucson, AZ, 85721, USA

HIGHLIGHTS

- Ring-type collapse in the nonlinear Schrödinger equation is not self-similar.
- Multibump solutions may be used as a basis for approximating dynamics.
- Rescaled ring radii shrink and eventually peak collapse occurs instead.
- Ring profiles with vortex or vectorial character can persist in modified systems.

ARTICLE INFO

Article history:
Received 14 June 2013
Received in revised form
28 May 2014
Accepted 26 June 2014
Available online 4 July 2014
Communicated by Y. Nishiura

Keywords:
Nonlinear Schrödinger equation
Self-similarity
Blowup

ABSTRACT

The critical nonlinear Schrödinger equation (NLS) possesses nearly self-similar ring profile solutions. We address the question of whether this profile is maintained all the way until the point of singularity. A perturbative analysis of the rescaled PDE and the resulting self-similar profile uncover slow dynamics that eventually drive the ring structure to the classical peak-shaped collapse instead. A numerical scheme capable of resolving self-similar behavior to high resolutions confirms our analysis. We also consider ring-type blowup arising either from azimuthally polarized solutions of a coupled NLS system or as vortex solutions of the usual NLS. In this case, the ring profile is maintained up to the time of singularity.

1. Introduction

The cubic nonlinear Schrödinger equation (NLS)

$$i\frac{\partial \psi}{\partial t} + \Delta\psi + |\psi|^2\psi = 0, \quad \psi : \mathbb{R}^d \times \mathbb{R}^+ \to \mathbb{C}, \tag{1}$$

arises in nonlinear optics, fluid dynamics, plasma physics, and Bose–Einstein condensates. In the context of propagation of optical pulses, ψ describes the envelope of the electric field, where t is the direction of propagation and $d = 2$ is the dimension of the transverse coordinates.

When $d = 1$, the cubic NLS is integrable and solutions are globally well-defined (see, e.g., [1]). For dimensions $d \geq 2$, it is well known that solutions may not exist for all times, with singular behavior $\|\psi\|_\infty \to \infty$ occurring at a finite time $t = T$. For d strictly larger than 2, this can occur in a precisely self-similar fashion

$$\psi_{ex}(x,t) = \frac{1}{\sqrt{2a(T-t)}} e^{i\log(T-t)/2a} Q\left(\frac{|x|}{\sqrt{2a(T-t)}}\right), \tag{2}$$

where Q and the scaling parameter $a > 0$ are determined as a nonlinear eigenvalue problem [1]. The potentially complex-valued function Q is the collapse profile in similarity variables, and is in general non-unique.

The nature of singular solutions in the critical dimension $d = 2$ is much more subtle. The rate constant a in ψ_{ex} vanishes as $d \downarrow 2$, making Eq. (2) meaningless. A series of papers [2–4] clarified that collapse may be nearly self-similar in the following sense: the solution profile (in similarity variables) evolves adiabatically which leads to a small double-logarithmic correction in the blowup rate. Originally the profiles that were considered were strictly radially symmetric and monotone, and asymptote to the ground state solution of the *Townes* equation

$$R_{rr} + \frac{1}{r}R_r - R + R^3 = 0, \quad R_r(0) = 0$$

* Corresponding author.
E-mail addresses: jallenf@math.arizona.edu (J. Allen-Flowers), kglasner@math.arizona.edu (K.B. Glasner).

http://dx.doi.org/10.1016/j.physd.2014.06.009
0167-2789/

as the singularity time is approached. Subsequent work has verified this in a rigorous fashion [5,6], and experimental data were found to be consistent with the Townes profile [7].

Non-monotone self-similar profiles have also been discovered. These were first noted by Budd et al. [8] in numerical experiments for supercritical dimensions $d > 2$. In these solutions, the amplitude concentrates on a ring (or rings) whose radius shrinks to zero. A formal asymptotic description of the self-similar profiles was given in [9]. A rigorous proof of existence and uniqueness of the profile equation was later provided by Rottschäfer and Kaper [10]. Although we are primarily concerned with the dynamics in the critical dimension $d = 2$, we employ the self-similar solutions for $d > 2$ as the basis for a perturbative analysis.

Numerical experiments of ring-type solutions for the critical dimension $d = 2$ were subsequently conducted by Fibich et al. [11]. These revealed that near the singularity, solution profiles may indeed be non-monotone in the radial variable, and the behavior appears to be self-similar with a rate which is exactly a square root. More specifically, they observe "single bump" profiles which correspond to intensity maxima on two dimensional rings of ever shrinking radius. Their numerical results suggest that the ring structure is maintained all the way until the singularity; however, there is currently no rigorous proof to support this. They concede that strictly self-similar solutions would be unphysical, as they must have infinite power (see 2.4). This leaves open two questions:

1. For physical initial data, does any part of the solution converge to a self-similar profile?
2. Does the ring profile really persist until the time of singularity, or does it eventually transition to different behavior?

In this paper we address both questions with formal asymptotic analysis confirmed by careful numerical experiments. As with the original case of monotone blowup profiles in the critical dimension, the dynamic behavior is not strictly self-similar. We also find that ring solutions represent only an intermediate stage in the blowup dynamics, and eventually transition to monotone profiles.

This paper is organized as follows. In Section 2 we review some of the theoretical aspects of blowup and self-similarity for Eq. (1). In Section 3, we generalize the calculation of LeMesurier et al. [4] to the case of non-monotone blowup profiles. We present an asymptotic argument that suggests the location of the ring radius (in stretched variables) is not constant, but that exponentially slow dynamics eventually drive it towards the origin. We verify our analysis quantitatively using a numerical method suitable for resolving self-similar solutions to high resolution. In Section 4, we consider a modified system where the Laplacian in Eq. (1) is replaced by the vector Laplacian, which arises from azimuthally polarized solutions of a coupled system. We find there that similar ring-type blowup occurs but does not transition to a different behavior as the singularity is approached.

2. Singular solutions of the critical and supercritical NLS

We begin by reviewing analytic properties of the NLS and some of its known solutions. Attention will be focused on the radially symmetric case where Eq. (1) becomes

$$i\psi_t + \psi_{rr} + \frac{d-1}{r}\psi_r + |\psi|^2\psi = 0. \tag{3}$$

For reasons that will be clear later, the dimension d will take non-integer values.

Eq. (3) has two important conserved quantities: the L^2 norm (power)

$$N(t) = \int_0^\infty |\psi|^2 r^{d-1} dr \equiv N(0), \tag{4}$$

and the Hamiltonian

$$H(t) = \int_0^\infty \left(|\nabla\psi|^2 - \frac{1}{2}|\psi|^4\right) r^{d-1} dr \equiv H(0). \tag{5}$$

A necessary condition for blowup is that the initial power exceeds some threshold value, $N(0) > N_c$; a sufficient condition is that the Hamiltonian is negative [11].

A particular solution of Eq. (3) comes from separation of variables, $\psi(r,t) = e^{it}R(r)$, where $R(r)$ satisfies

$$R_{rr} + \frac{1}{r}R_r - R + R^3 = 0, \quad R_r(0) = 0,\ R(\infty) = 0. \tag{6}$$

This problem was studied in [12]. It admits a sequence of solutions R_k, $k = 0, 1, 2, \ldots$ which can be arranged in order of increasing power, where R_k has k zeros and $k+1$ turning points. The lowest power nontrivial solution of Eq. (6), R_0, is referred to as the ground state or Townes profile, which contains exactly the critical power for blowup, $N_c \approx 11.69$. Each solution R_k decays exponentially and monotonically for large r.

2.1. Similarity ansatz

For singular solutions, we expect there to be a length scale $L(t)$ that tends to zero at some finite time T. In the case of self-similar blowup, L is a characteristic width of the solution, while the maximum amplitude scales as L^{-1}. It is useful to work in similarity variables

$$\tau = \int_0^t L^{-2}(s)ds, \qquad \xi = \frac{r}{L(t)}, \tag{7}$$

so that the singularity is pushed to $\tau = \infty$ and the characteristic length scale remains finite. The dependent variable is written as

$$\psi(r,t) = \frac{1}{L(t)}u(\tau,\xi), \tag{8}$$

where

$$iu_\tau + u_{\xi\xi} + \frac{d-1}{\xi}u_\xi + ia\,(\xi u)_\xi + |u|^2u = 0, \tag{9}$$

and where the dynamic rate parameter $a = a(\tau)$ is defined by $a = -LL_t = -L^{-1}L_\tau$.

Note that if a is a constant, one has an exactly square-root blowup rate, $L = [2a(T-t)]^{1/2}$. We can then look for solutions to Eq. (9) of the form $u(\tau,\xi) = e^{i\tau}Q(\xi;a)$, where Q satisfies

$$Q_{\xi\xi} + \frac{d-1}{\xi}Q_\xi - Q + ia\,(\xi Q)_\xi + |Q|^2Q = 0 \tag{10}$$

subject to the conditions

$$Q_\xi(0) = 0, \qquad \lim_{\xi\to\infty} Q(\xi) = 0. \tag{11}$$

For $d > 2$, the value of a is determined along with Q as a nonlinear eigenvalue problem. Together, a, L, and Q form the explicit blowup solutions $\psi_{ex}(r,t)$ from Eq. (2). We remark that the frequency in the phase factor $e^{i\tau}$ is arbitrary; a different choice would simply lead to a rescaled problem equivalent to (10)–(11).

Although (9) is valid for any smooth, positive choice of $L(t)$, in the spirit of similarity solutions L is chosen to renormalize the solution and alleviate the singular behavior. In particular, we want the maximum of $|u|$ to be a constant. For the solutions studied in Section 3, this is guaranteed by the particular choice

$$L = \sqrt{\frac{3}{2}}\left(\sup_x |\psi(x)|\right)^{-1}. \tag{12}$$

The prefactor is chosen to be consistent with steady state solutions for the supercritical case (c.f. Section 2.3).

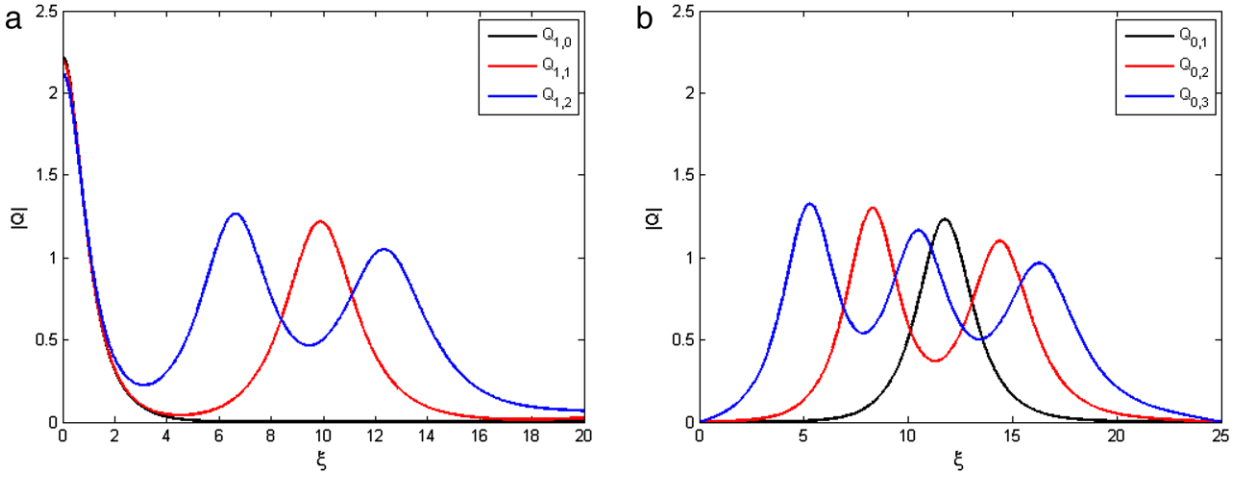

Fig. 1. Solutions of Eq. (10); (a) $|Q_{k,j}|$ for $k = 1, j = 0, 1, 2$; (b) $|Q_{k,j}|$ for $k = 0, j = 1, 2, 3$.

2.2. Monotone profiles in the supercritical case

Monotone solutions to (10)–(11) exist and are unique [13,14]. In particular, for $2 < d < 4$ there exists a smooth monotone relation $a = a_0(d)$, with its inverse denoted as $d = d_0(a)$. In [4], it was established that the asymptotics of this relation for $d \to 2$ is beyond all orders (in fact exponentially small in the parameter a) in the sense that

$$\left(\frac{\mathrm{d}}{\mathrm{d}a}\right)^p (d_0(a) - 2)\Big|_{a=0} = 0 \quad \text{for all } p = 0, 1, 2, \ldots.$$

In fact, the limit of the corresponding monotone solutions as $d \to 2$ is exactly the ground state solution to (6). This does not represent a self-similar profile for $d = 2$ since (2) is meaningless for $a = 0$.

To analyze collapse in the critical dimension, LeMesurier et al. [4] supposed that the solution was always near one of the monotone supercritical profiles $Q(\xi; a)$. In this case, a is regarded as slowly varying (with respect to the similarity time variable τ). This allows a perturbative solution for small a to be sought, leading to an ordinary differential equation for a of the form $a_\tau \sim -C(d_0(a) - 2)$. The exponential smallness of $d_0(a) - 2$ means that the solution profile changes very slowly and the blowup rate has a correspondingly subtle log–log correction.

2.3. Multibump profiles

For dimension strictly larger than two, there are many non-monotone self-similar profiles [8–10]. For $a \ll 1$ and d very near to 2, Eq. (10) can be regarded as a singular perturbation of Eq. (6). For each $R_k(r)$, $k = 0, 1, 2 \ldots$, there is a corresponding sequence $Q_{k,j}(\xi; a(d))$, $j = 0, 1, 2 \ldots$ such that $Q_{k,j}$ has $(k+j)$ local maxima. In [10], Rottschäfer and Kaper rigorously proved the existence and uniqueness of these solutions for $k = 1, j = 0, 1, \ldots$ when a is sufficiently small. Although their paper does not explicitly address the case of $k = 0, j = 1$, which is the main focus of the present paper, their techniques can still be used to show existence in this instance. Numerical examples of these solutions are shown in Fig. 1.

A detailed asymptotic analysis of Eq. (10) for multibump profiles was given by Budd [9]. Here we summarize the relevant results from that paper which will be utilized in Section 3.

To understand how these multibump solutions arise, it is convenient to write $P = e^{ia\xi^2/4}Q$ and study the equation for P:

$$P_{\xi\xi} + \frac{d-1}{\xi}P_\xi - P + \frac{a^2\xi^2}{4}P - ia\frac{d-2}{2}P + |P|^2P = 0. \tag{13}$$

As in the case of monotone profiles, for each $Q_{k,j}$ there is an invertible relationship between the nonlinear eigenvalue a and the dimension d, which may be written $d = d_0(a)$. It turns out that $d_0(a) - 2$ is exponentially small in a; specifically for the single bump solutions $Q_{0,1}$, the estimate

$$d_0(a) - 2 \sim \frac{3}{a}e^{-(2\pi/3-\sqrt{3/4})/a}, \quad a \to 0, \tag{14}$$

may be derived [9]. This implies that the coupling between real and imaginary parts of P is very weak. Writing

$$P = A + iB,$$

then to all algebraic orders in a we have

$$A_{\xi\xi} + \frac{1}{\xi}A_\xi - A + \frac{a^2\xi^2}{4}A + A^3 = 0, \tag{15}$$

which is readily seen as a perturbation of Eq. (6) in the region where $a\xi \ll 1$. Furthermore, without loss of generality $P(0) \in \mathbb{R}$, so that the imaginary part is in fact exponentially small in a.

It was shown in [15] that all solutions of (15) decay when a is nonzero. Therefore peaks of the multibump solutions necessarily occur where $\xi = O(1/a)$. To derive the shape and location of the peaks, one can write

$$s = \xi - \kappa/a,$$

and look for solutions to (10) of the form

$$Q = e^{-i\kappa s/2}\left(S_0(s) + aS_1(s) + \cdots\right).$$

The leading order term satisfies a scaled version of Duffing's equation,

$$S_{0,ss} - \left(1 - \kappa^2/4\right)S_0 + S_0^3 = 0$$

with solution given by

$$S_0(s) = \sqrt{2(1-\kappa^2/4)}\,\mathrm{sech}\left(\sqrt{1-\kappa^2/4}s\right).$$

For the single-peak solution $Q_{0,1}$, the value of κ is found from a consistency condition at the next order of the expansion to be $\kappa = 1 + O(a^2)$, so that

$$|Q_{0,1}(\xi)| \sim \sqrt{\frac{3}{2}}\,\mathrm{sech}\left(\sqrt{\frac{3}{4}}(\xi - 1/a)\right), \quad a \to 0. \tag{16}$$

Multibump solutions of (13) were studied rigorously in the work of Rottschäfer and Kaper [10]. In particular, they establish the existence and uniqueness of the one bump solution $Q_{0,1}(\xi)$ over some range $0 < a < a_{\max}$.

2.4. Collapsing ring solutions

In [11], Fibich et al. presented numerical simulations of the critical dimension NLS where the blowup appears to occur on a ring whose radius tends to zero, rather than at the origin. They show that if $\psi(r,t)$ takes an asymptotic self-similar form

$$\psi(r,t) \sim \psi_G = \frac{1}{L(t)} G(\xi) e^{i\tau + i(L_t/L)(r^2/4)}, \tag{17}$$

then one necessarily has

$$G_{\xi\xi} + \frac{1}{\xi} G_\xi - G + \frac{a^2\xi^2}{4} G + G^3 = 0 \tag{18}$$

and $L(t)$ must have exactly a square root behavior.

It is worth noting that the large-ξ asymptotics of G are [11]

$$G(\xi) \sim \frac{c_G}{\xi} \cos\left(\frac{a}{4}\xi^2 - a^{-1}\log\xi + c_2\right), \quad \xi \to \infty$$

where c_g and c_2 depend on the global structure. The tail of G decays algebraically and in particular the power integral $\int_0^\infty |G|^2 \xi\, d\xi$ is not finite. As a consequence, any initial conditions which generate a solution asymptotic to G everywhere must also have infinite power. In [11], it is supposed that for general initial conditions which generate ring-type collapse, only the part of the solution in the large amplitude ring-region is given by (17).

Fibich et al. [11] also tested the stability of collapsing ring solutions numerically. They determine that the one-ring solution is stable with respect to radially-symmetric perturbations, but is unstable for non-radial initial conditions. In the case of multi-ring solutions (based off of the functions $Q_{k,j}$), only the innermost ring will continue to blow up, while the outer rings become wider. Therefore, the one-ring solution is an attractor for a wide range of radially-symmetric initial conditions, but is unstable with respect to symmetry-breaking perturbations.

3. Dynamics of ring solutions in the critical case

In this section, we propose a perturbative ansatz for solutions which collapse with one-ring profiles. We suppose that the rescaled profiles that satisfy (9) do not approach a steady state, but rather evolve slowly, at least when a is small. In this respect, our calculation is a generalization of LeMesurier et al. [4]. The results are then checked numerically, showing that ring profiles are indeed dynamic and eventually transition to monotone profiles.

It is convenient to reformulate Eq. (9) by the substitution $V(\tau,\xi) = e^{-i\tau + ia\xi^2/4} u$, which in the critical dimension $d = 2$ leads to

$$iV_\tau + V_{\xi\xi} + \frac{1}{\xi} V_\xi - V + \left(a^2 + a_\tau\right)\frac{\xi^2}{4} V + |V|^2 V = 0. \tag{19}$$

Note that the analogous substitution for the self-similar profiles, $P = e^{ia\xi^2/4} Q$, leads to Eq. (13).

3.1. Expansion around multibump solutions

In order to determine the evolution of a ring-type solution, we suppose that solutions of (9) are well-approximated by the family of single bump solutions $u \approx e^{i\tau} Q_{0,1}(\xi; a)$, since each member of this family has a unique ring radius $\xi_{\max} \approx 1/a$. We emphasize that even though each profile corresponds to a steady solution of (13) in a particular dimension $d = d_0(a)$, the dynamics of u are only occurring in dimension $d = 2$ here. The evolution problem then reduces to determining the slow-scale dynamics of $a(\tau)$.

In terms of the reformulated Eq. (19), the solution is approximated as

$$V(\tau,\xi) = P_{0,1}(\xi; a(\tau)) + W(\xi,\tau), \tag{20}$$

where $P_{0,1}(\xi; a) = e^{ia\xi^2/4} Q_{0,1}(\xi; a)$ solves (13). The correction W is assumed to be small; in particular

$$W = \mathcal{O}(\exp(-1/a)), \quad a \to 0. \tag{21}$$

Let us briefly explain the philosophy behind the choice of approximation. One can think of the family of profiles

$$\mathcal{M} = \left\{P_{0,1}(\xi; a) | 0 \le a \le a_{\max}\right\} \tag{22}$$

as a kind of "slow" manifold of the evolution equation (19). In particular, using (13) note that

$$\begin{aligned}\frac{\partial}{\partial\tau} P_{0,1} &= i\left(\frac{d_0(a)-2}{\xi}(P_{0,1})_\xi - a_\tau \frac{\xi^2}{4} P_{0,1}\right) \\ &\quad + \left((P_{0,1})_a a_\tau - a\frac{d_0(a)-2}{2} P_{0,1}\right).\end{aligned} \tag{23}$$

The terms proportional to $d_0(a) - 2$ are necessarily $\mathcal{O}(\exp(-1/a))$. We also find, *a posteriori*, that a_τ is also proportional to $d_0(a) - 2$. The dynamics of $a(\tau)$ result from projecting the dynamics of (19) onto $\mathcal{M}$.

Putting (20) into (19) and using (13) gives

$$\begin{aligned}&W_{\xi\xi} + \frac{d_0(a)-1}{\xi} W_\xi - W + \frac{a^2\xi^2}{4} W + P_{0,1}^2 W^* + 2|P_{0,1}|^2 W \\ &= \frac{d_0(a)-2}{\xi}\left((P_{0,1})_\xi + W_\xi\right) \\ &\quad - \frac{a_\tau \xi^2}{4}(P_{0,1} + W) - ia\frac{d_0(a)-2}{2} P_{0,1} - iW_\tau \\ &\quad - i(P_{0,1})_a a_\tau - 2P_{0,1}|W|^2 - P_{0,1}^* W^2 - |W|^2 W.\end{aligned} \tag{24}$$

Note that the left-hand side of this equation is the linearized operator from Eq. (13) acting on W. Since we are interested in leading order behavior only, terms which are products of exponentially small quantities will be neglected. The resulting leading order equation for W is

$$\begin{aligned}&W_{\xi\xi} + \frac{d_0(a)-1}{\xi} W_\xi - W + \frac{a^2\xi^2}{4} W + 2|P_{0,1}|^2 W + P_{0,1}^2 W^* \\ &= -i\left((P_{0,1})_a a_\tau + a\frac{d_0(a)-2}{2} P_{0,1}\right) \\ &\quad - \left(a_\tau \frac{\xi^2}{4} P_{0,1} - \frac{d_0(a)-2}{\xi}(P_{0,1})_\xi\right).\end{aligned} \tag{25}$$

We separate this into real and imaginary parts as $W = S + iT$ and $P_{0,1} = A + iB$. Recall from Eq. (13) and the discussion thereafter that B is exponentially small in a, so at leading order P is approximated by its real part. The equations for S and T are to leading order

$$\begin{aligned}&S_{\xi\xi} + \frac{d_0(a)-1}{\xi} S_\xi - S + \frac{a^2\xi^2}{4} S + 3A^2 S \\ &= -\left(a_\tau \frac{\xi^2}{4} A - \frac{d_0(a)-2}{\xi} A_\xi\right)\end{aligned} \tag{26}$$

$$\begin{aligned}&T_{\xi\xi} + \frac{d_0(a)-1}{\xi} T_\xi - T + \frac{a^2\xi^2}{4} T + A^2 T \\ &= -\left(a_\tau A_a + a\frac{d_0(a)-2}{2} A\right).\end{aligned} \tag{27}$$

Eq. (26) is solvable with a general inhomogeneous right-hand side, but (27) is not [4]. Eq. (27) is of the form $\mathcal{L}T = f(\xi)$ where the self

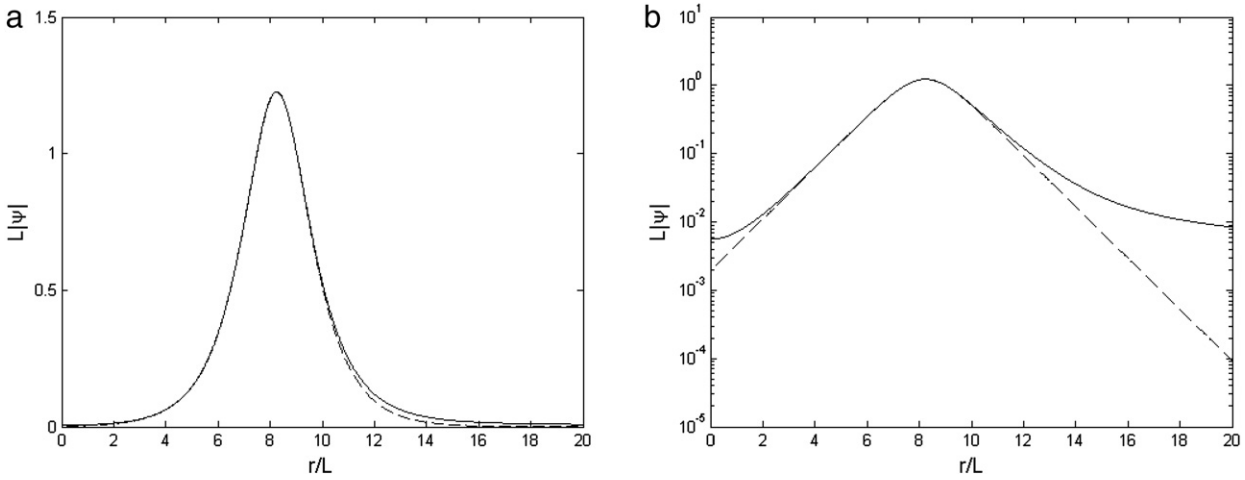

Fig. 2. (a) Solution of (3) when $\max|\psi(r,t)| = 1.22 \times 10^{10}$, normalized by Eq. (12) (solid), and the asymptotic solution (16) (dashed). The initial condition is $\psi(r,0) = 12.2e^{-r^4}$, with power $N_0 = 25N_c$; (b) the same data plotted on a logarithmic scale.

adjoint (with respect to the radial L^2 inner product) operator $\mathcal{L}$ is defined as

$$\mathcal{L} = \frac{\partial^2}{\partial\xi^2} + \frac{d_0(a)-1}{\xi}\frac{\partial}{\partial\xi} - 1 + \frac{a^2\xi^2}{4} + A^2. \tag{28}$$

A Fredholm solvability condition for (27) arises in the usual way, but the nullspace can only be computed approximately. From Eq. (13),

$$\mathcal{L}P_{0,1} = ia\frac{d_0(a)-2}{2}P_{0,1} + B^2P_{0,1}, \tag{29}$$

so that

$$\mathcal{L}A = -a\frac{d_0(a)-2}{2}B + B^2A. \tag{30}$$

Observe both terms on the right are exponentially small in a. Therefore taking the inner product of (27) with A instead of the exact eigenfunction will remain consistent with the desired order of approximation. This leads to

$$\begin{aligned} &-a\frac{d_0(a)-2}{2}\int_0^\infty B(\xi)T(\xi)\xi\,d\xi \\ &= -\int_0^\infty A(\xi)\left(a_\tau A_a + a\frac{d_0(a)-2}{2}A\right)\xi\,d\xi. \end{aligned} \tag{31}$$

The integrals are each $\mathcal{O}(\exp(-1/a))$, but the one on the left is multiplied by another exponentially small factor. The dominant term is therefore the integral on the right, and this leads to an expression for the dynamics

$$a_\tau = -a(d_0(a)-2)\frac{\int A^2\xi\,d\xi}{\int (A^2)_a\xi\,d\xi}. \tag{32}$$

Note that a_τ is proportional to $d_0(a)-2$, which is exponentially small in a as claimed. The dominant contribution to the integrals comes from the ring region of A, where (from Eq. (16))

$$A \approx |P(\xi;a)| \sim \sqrt{\frac{3}{2}}\operatorname{sech}\left(\sqrt{\frac{3}{4}}(\xi - 1/a)\right), \quad a \to 0. \tag{33}$$

From this we can explicitly compute the main contribution to the integrals in (32):

$$\begin{aligned} &\int_0^\infty A^2\xi\,d\xi \approx 2\log\left(1+e^{\sqrt{3}/a}\right), \\ &\int_0^\infty \left(A^2\right)_a\xi\,d\xi \approx -\frac{2\sqrt{3}e^{\sqrt{3}/a}}{a^2\left(1+e^{\sqrt{3}/a}\right)}. \end{aligned} \tag{34}$$

The most significant consequence of (32) is that a_τ is increasing, in contrast to the slow dynamics of monotone profiles. Since the location of the peak $\xi_{\max}$ scales as $1/a$, this means that (even in rescaled variables) the peak location proceeds inward, rather than remaining constant as asserted in [11]. Note the opposite result would have been counterintuitive, since the ring would increase in radius, and power contained in the ring would have to increase, which would require radiation of energy from $\xi = +\infty$.

Another consequence of (32) is that eventually a becomes so large that the qualitative reliability of the approximation becomes doubtful. Two natural possibilities are that either the profile remains ring-like but is not close to the multibump profile $Q_{0,1}$, or the profile transitions to a completely different shape. We explore this subsequently through simulation.

3.2. Numerical experiments

The slow dynamics which we have described analytically present considerable challenges for numerical verification. We have developed a code which deals with both small length- and time-scales, capable of integrating the solution to amplification factors of at least 10^{13}. The details of the algorithm are outlined in the Appendix.

Fig. 2 shows a typical solution as it approaches the singularity, plotted in scaled variables. For comparison, we have also plotted the asymptotic solution from Eq. (16). The agreement is good in the peak region, but as Fig. 2(b) shows, there is a mismatch in the tail.

We have found that for a wide variety of initial conditions, a similar agreement between simulations and our ansatz (20) occurs after a transient period of time. Even for monotone initial conditions such as the "super-Gaussian" $\psi(r,0) \propto e^{-r^4}$, the solution developed a non-monotone ring structure and proceeded to collapse with the $Q_{0,1}$ profile, rather than the monotonic $Q_{1,0}$ profile.

The length scale $L(t)$ can be extracted directly from the numerics via Eq. (12). Denoting $r_{\max} = \operatorname{argmax}|\psi(r,\cdot)|$, the location of the peak in scaled variables, $\xi_{\max}$, can then be calculated as $\xi_{\max} = r_{\max}/L$. From (16), we know this location to be $\xi_{\max} = 1/a$, thus we can determine a as

$$a = \frac{L}{r_{\max}}. \tag{35}$$

Once $L(t)$ is computed, Eq. (7) can be integrated numerically to evaluate the scaled time variable τ.

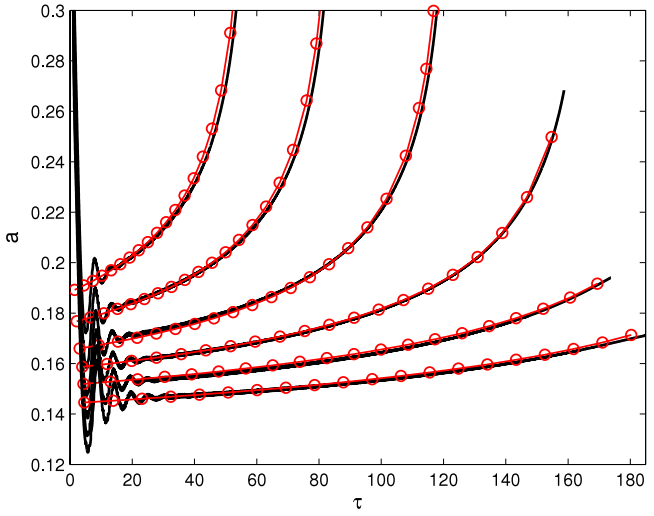

Fig. 3. Numerical (solid) and asymptotic (circles) calculation of the dynamic rate parameter a. The initial condition used to solve (3) numerically is $\psi(r,0) = Ce^{-r^4}$, with C being chosen to adjust the initial power to values between $13N_c$ and $18N_c$. Higher power corresponds to smaller values of $a(0)$.

Fig. 3 shows the results of running six simulations with initial condition $\psi(r,0) = Ce^{-r^4}$, where C is chosen so that the initial power N_0 ranges from $13N_c$ to $18N_c$. After some transient oscillations, a single ring profile forms, with some of the power being radiated away to $r = \infty$. Varying the initial power provides control over the initial ring radius, and in particular corresponds to different initial values of $a(\tau)$. The solution was integrated until either the ring transitioned to a monotone profile ($N_0/N_c = 13-15$), or a maximum value of 1.35×10^{13} was reached ($N_0/N_c = 16-18$). We have also used initial conditions to mimic the ansatz (20) of the form $\psi(r,0) = \sqrt{\frac{3}{2}}\operatorname{sech}\left(\sqrt{\frac{3}{4}}(\xi - 1/a)\right)$ with similar results.

The initial value $a(0)$ is extrapolated from the numerical solution using linear regression from the data for $0 \le \tau \le 40$. This provides the initial condition for the ordinary differential equation (32) for $a(\tau)$, which is solved numerically using Eqs. (14) and (34). There is considerable agreement between the simulation of the full equation and reduced dynamics, especially when $a(\tau)$ is small. The agreement becomes worse where $a = \mathcal{O}(1)$, which would be expected of a perturbative approximation.

Note that the initial power must be chosen in a very particular range for meaningful comparisons. If N_0 is too high, the dynamics will be too slow to observe, even when the solution reaches a peak magnitude of 10^{13}. This is the case in [11], where ring profiles appeared to be static. If N_0 is too low, the transition to a monotone profile will happen too quickly and the analysis leading to Eq. (32) is not valid.

We have found in all cases, there is a rapid transition (in contrast to the slow motion of (32)) from ring-shaped to monotonic profiles when the computed value of $a \approx .5$. This transition is captured in Fig. 4. As $a(\tau)$ continues to increase, the location of the peak in scaled variables continues to decrease, until eventually the peak is forced onto the origin.

4. A coupled NLS system

To account for the effects of field polarization in optical propagation, a two-component system of coupled nonlinear Schrödinger equations is considered [16,17]. These describe the amplitude of the envelope of the transverse field components, (ψ_1, ψ_2). With a particular set of constitutive parameters, this system has the form

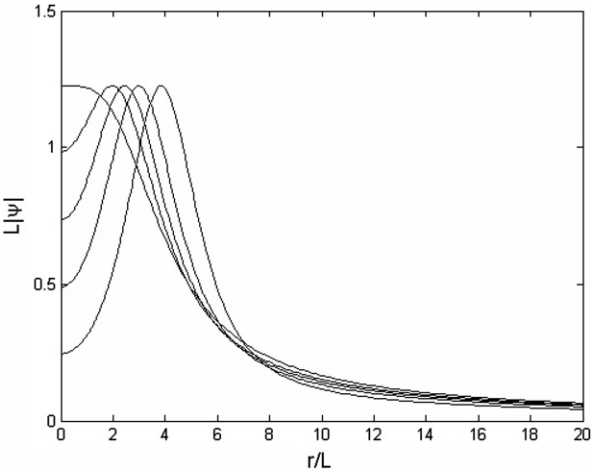

Fig. 4. The solution of NLS (3) with initial condition $\psi(r,0) = 9.62e^{-r^4}$, with $N_0 = 15.6N_c$, plotted in scaled variables. The solution is shown at times when $\max|\psi| = 5.38 \times 10^{11}$, 3.4×10^{12}, 6.28×10^{12}, 8.77×10^{12}, and 1.23×10^{13}.

$$i\frac{\partial \psi_1}{\partial t} + \Delta\psi_1 + (|\psi_1|^2 + |\psi_2|^2)\psi_1 = 0, \tag{36}$$

$$i\frac{\partial \psi_2}{\partial t} + \Delta\psi_2 + (|\psi_1|^2 + |\psi_2|^2)\psi_2 = 0. \tag{37}$$

In two transverse dimensions, one can look for radial solutions which have azimuthal polarization, that is solutions of the form $(\psi_1, \psi_2) = \psi(r,t)\hat{\theta}$. This leads to a modified version of the radial NLS equation (3),

$$i\psi_t + \psi_{rr} + \frac{1}{r}\psi_r - \frac{1}{r^2}\psi + |\psi|^2\psi = 0. \tag{38}$$

The spatial operator in (38) now contains the extra term $-\psi/r^2$, and is the radial component of the vector Laplacian. To enforce continuity of the underlying field, one requires $\psi(0,t) = 0$ at the origin, in contrast to the Neumann condition for Eq. (3). It is interesting to note that this prohibits any collapse (self-similar or not) which has an intensity maximum at the origin. As a consequence, no transition to monotone blowup profiles is possible.

Eq. (38) was studied by Fibich et al. [18] in a slightly different context. In that case, "vortex" solutions of (1) having the form $\psi = \exp(im\theta)g(r,t)$ were considered. For $m = 1$, this leads to (38). It was shown numerically that collapsing ring solutions exist in this case. Just as with (3), exactly self-similar solutions having finite power do not exist in dimension $d = 2$.

4.1. Multibump solutions for the modified operator

A modification of the problem (10),

$$\tilde{Q}_{\xi\xi} + \frac{d-1}{\xi}\tilde{Q}_\xi - \frac{1}{\xi^2}\tilde{Q} - \tilde{Q} + ia\left(\xi\tilde{Q}\right)_\xi + |\tilde{Q}|^2\tilde{Q} = 0, \tag{39}$$

$$\tilde{Q}(0) = 0, \qquad \lim_{\xi\to\infty}\tilde{Q}(\xi) = 0 \tag{40}$$

was studied by Shi [19], where an asymptotic analysis akin to [9] was developed. A similar set of multibump profiles exists, with slight modifications to the underlying structure. Significantly, the single-peak solution $\tilde{Q}_{0,1}$ behaves as

$$|\tilde{Q}_{0,1}| \sim \sqrt{\frac{3(2-\kappa^2)}{2}}\operatorname{sech}\left(\sqrt{\frac{3(2-\kappa^2)}{4}}(\xi - \kappa/a)\right), \quad a \to 0, \tag{41}$$

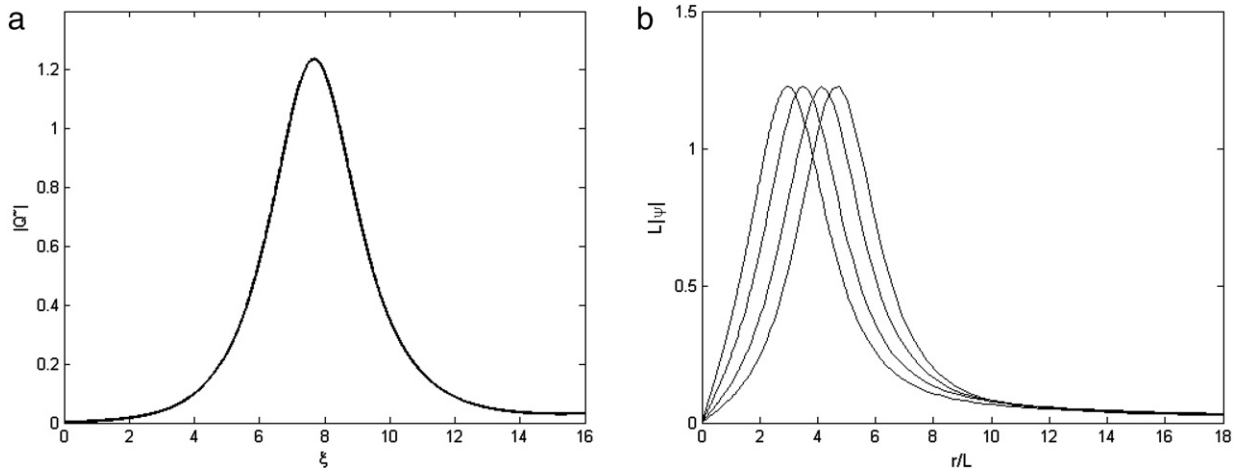

Fig. 5. (a) Typical solution of (39); (b) numerical solution of Eq. (38), at times when max $|\psi| = 10^3$, 10^6, 10^9, and 10^{12}.

where the scaled peak location is now a function of a given by

$$\kappa = \sqrt{\frac{1}{2}\left(1 + \sqrt{1 - 8a^2}\right)}. \tag{42}$$

There is a similar relationship $d = \tilde{d}_0(a)$, which leads to

$$d - 2 = \frac{3(2-\kappa^2)}{a} e^{-\lambda(a)/a}, \tag{43}$$

with

$$\lambda(a) = 4\int_{\kappa/2}^{x_0} \sqrt{1 + \frac{a^2}{4s^2} - s^2}\, ds,$$

where x_0 is the zero of the integrand. The complete details of the calculation can be found in [19].

4.2. Ring profile dynamics

The analysis in Section 3 can be repeated for Eq. (38) in precisely the same manner. Since there is no difference in the underlying structure of the linearized problem, the resulting dynamical equation for the parameter $a(\tau)$ looks similar to (32),

$$a_\tau = -a(\tilde{d}_0(a) - 2)\frac{\int \tilde{A}^2 \xi\, d\xi}{\int (\tilde{A}^2)_a \xi\, d\xi}, \tag{44}$$

where now $\tilde{A} = |\tilde{Q}_{0,1}|$. The integrals in (44) are modified to

$$\begin{aligned} \int_0^\infty \tilde{A}^2 \xi\, d\xi &\approx 2\log\left(1 + e^{g\sqrt{3}/a}\right) \\ \int_0^\infty \left(A^2\right)_a \xi\, d\xi &\approx -\frac{2\sqrt{3}e^{g\sqrt{3}/a}}{a^2\left(1 + e^{g\sqrt{3}/a}\right)}\left(g - a g_a\right), \end{aligned} \tag{45}$$

where $g = g(a) = \sqrt{2\kappa^2 - \kappa^4}$. The sign of $da/d\tau$ is positive when a is small, signifying a general trend for the profiles to contract toward the origin.

4.3. Numerical tests

A numerical study of (38) and (39) was conducted, similar to that of Section 3.2. A typical single peak solution of (39) is shown in Fig. 5(a). Dynamical solutions of (38) in scaled variables are shown in Fig. 5(b) using the initial condition $\psi(r, 0) = 15.41 r^2 e^{-r^4}$. We find that the profile continually steepens near the origin, without any qualitative change in shape.

Eq. (41) shows that the amplitude of $\tilde{Q}_{0,1}$ is no longer independent of a. The length scale L that leads to Eq. (39) must be modified accordingly,

$$L = \sqrt{\frac{3(2-\kappa^2)}{2}}\psi_{\max}^{-1}. \tag{46}$$

The quantity $a(\tau)$ can be extracted from the numerics, in the same spirit as in Section 3.2, by solving

$$\frac{r_{\max}}{L} = \frac{\kappa}{a}$$

which yields

$$a = \sqrt{\frac{3}{2}}\frac{\sqrt{\rho^2 - 6}}{\rho^2 - 3},$$

where $\rho = \psi_{\max} r_{\max}$. Once a is known, L can be calculated and Eq. (7) can be integrated for the scaled time τ.

Fig. 6 shows the results of running 4 simulations with initial condition $\psi(r, 0) = Cr^2 e^{-r^4}$, where $C = 16.16$, 16.88, 17.57, and 18.23. Changing the value of C allows control over the initial value for $a(\tau)$, with higher C values corresponding to lower $a(0)$. In each case, the solution was integrated until $\psi_{\max} = 1.35 \times 10^{13}$. As before, the initial value $a(0)$ is extrapolated from the numerical solution and used to solve Eq. (44) numerically, utilizing (43) and (45). We find good agreement with the asymptotic formula for reasonably small $a(\tau)$, but significant deviations for larger a.

4.4. Multi-dimensional stability

For completeness, we examine the stability of azimuthally polarized ring solutions $\psi(r, t)\hat{\theta}$ in the context of the full two-component system (36)–(37). For this, numerical simulations were conducted using a perturbed initial condition

$$(\psi_1, \psi_2) = \psi(r)\hat{\theta} + \boldsymbol{\psi}'(x, y). \tag{47}$$

The radial profile $\psi(r)$ was determined by solving (38) numerically until a roughly self-similar profile was formed. The perturbation $\boldsymbol{\psi}'$ was generated randomly using a Gaussian distribution.

The results are shown in Fig. 7. A modulation instability was noted for a variety of amplitudes of the perturbation, akin to the instability of collapsing rings in the regular NLS [11].

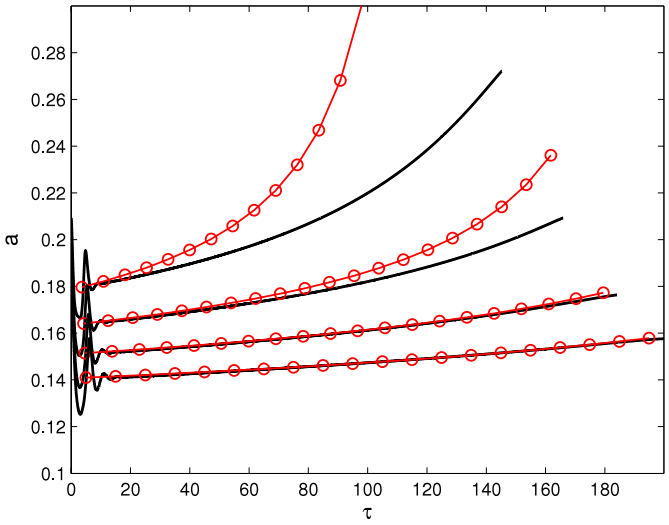

Fig. 6. Numerical (solid curves) and asymptotic (circles) calculation of $a(\tau)$ for the modified Eq. (38). The initial condition is $\psi(r, 0) = Cr^2e^{-r^4}$, with C taking values between 16.16 and 18.23. Compare with Fig. 3.

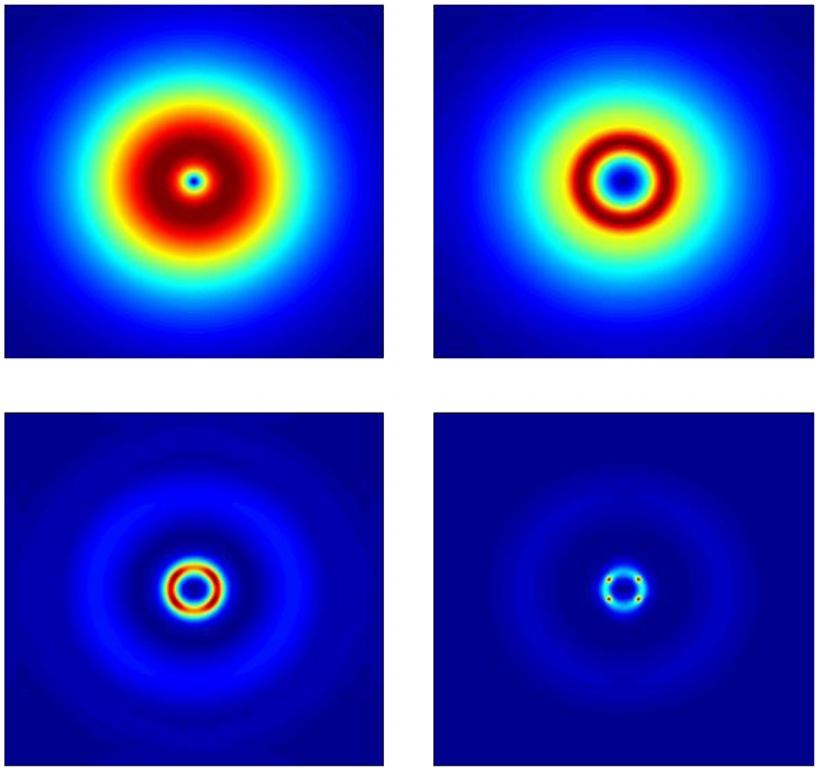

Fig. 7. Instability of an azimuthally polarized collapsing ring in the full coupled system (36)–(37). The color corresponds to the combined intensity $|\psi_1|^2 + |\psi_2|^2$. Collapse eventually occurs at points along the ring rather than maintaining the ring profile. (For interpretation of the references to colour in this figure legend, the reader is referred to the web version of this article.)

5. Conclusion

In this study, we investigated the dynamic behavior of collapsing ring solutions for the critical dimension nonlinear Schrödinger equation and its vector-Laplacian counterpart. Even though the self-similar profiles developed in [9] were for strictly supercritical dimension, we have shown their usefulness for approximating dynamic profiles in the critical dimension. It is not surprising that numerical studies such as in [11] would be misleading, as the ring dynamics can be exceptionally slow because of the beyond-all-orders character of the asymptotics. Another subtle aspect is that ring-type solutions may or may not represent the ultimate character of the collapse singularity, depending on the underlying spatial operator.

Our results rely heavily on formal asymptotic approximations and numerical confirmation. Although the analysis supports that the Townes profile is a universal attractor for critical blowup, a rigorous proof of this fact remains elusive. Our calculation states that the ring radius continues to decrease, but a more careful analysis is needed to determine what happens after the quantitative reliability of the approximation breaks down.

Our analysis could conceivably be generalized to other contexts. For example, multi-ring solutions can be regarded as essentially superpositions of ring profiles. In the nonlinear setting, interaction

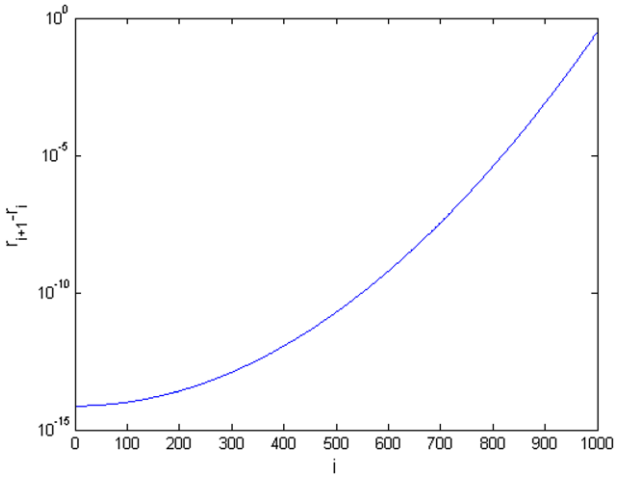

Fig. 8. Grid spacing for the numerical experiments in Section 3.2.

between individual rings is expected [20], leading to a reduced dynamical description of radial initial data.

From a practical point of view, it is significant that ring-type solutions can achieve very large power in the collapse region, in contrast to monotone collapse where power is always exactly the minimum critical power for blowup. To achieve transient but high intensity, it would be necessary to control or ameliorate azimuthal instability effects. This might have uses in, for example, high-power laser applications.

Acknowledgments

This work was supported by NSF award DMS-0807423 and Air Force Office of Scientific Research Multidisciplinary University Research Initiative (MURI) Grant FA9550-10-1-0561.

Appendix. Numerical method

Here we describe the method used to solve Eq. (3) numerically.

Spatial grid: In order to find a balance between computation time and accuracy, we employ a non-uniform stationary grid. The grid is constructed using $N+1$ points with $r_1 = 0$ and $r_{N+1} = L$, and the numerical solution lives at the center of the N cells. The cell spacing is

$$\begin{aligned}\Delta r_i &= r_{i+1} - r_i \\ &= L\left(\int_{s_i}^{s_{i+1}} e^{t^2} dt\right)\left(\int_0^M e^{t^2} dt\right)^{-1}, \quad i = 1, \ldots, N\end{aligned}$$

where $s_i = (i-1)M/N$ and M is an empirically chosen constant. For the numerical experiments in Section 3.2, $L = 5$, $N = 1000$, and $M = 5.6$. A plot of the grid spacing using these parameters is shown in Fig. 8(a). The Laplacian operator is discretized on this grid using second-order finite differences.

Time integration: The PDE is integrated in time according to the explicit update rule

$$\psi_{n+1} = \psi_n + i\Delta t_n \left(A\psi_{n+1} + |\psi_n|^2\psi_{n+1}\right),$$

where the matrix A is the discretized Laplacian operator. The time step Δt_n is changed after each update to reflect the analytical structure of the problem, so that $\Delta t_n = tol\,(\max_r |\psi_n|)^{-2}$. The value of tol is chosen to ensure that there is not a drastic change in Δt on the first time step, specifically $tol = \Delta t_0\,(\max_r |\psi(r,0)|)^2$. The time integration continues until either $\max_r |\psi| = 0.1\,(\min \Delta r)^{-1}$, or until $\operatorname{argmax}|\psi(r,\cdot)| = 0$.

Although this method does not conserve power, by using an initial time step on the order of 10^{-6}, power loss can be restricted to a few percent over the course of a blowup simulation.

References

[1] C. Sulem, P. Sulem, The Nonlinear Schrödinger Equation: Self-focusing and Wave Collapse, vol. 139, Springer Verlag, 1999.
[2] G. Fraiman, The asymptotic stability of the manifold of self-similar solutions in the presence of self-focusing, Zh. Eksp. Teor. Fiz. 88 (1985) 390–400.
[3] M. Landman, G. Papanicolaou, C. Sulem, P. Sulem, Rate of blowup for solutions of the nonlinear schrödinger equation at critical dimension, Phys. Rev. A 38 (1988) 3837–3843.
[4] B. LeMesurier, G. Papanicolaou, C. Sulem, P. Sulem, Local structure of the self-focusing singularity of the nonlinear Schrödinger equation, Physica D 32 (2) (1988) 210–226.
[5] M. Weinstein, The nonlinear Schrödinger equation — singularity formation, stability and dispersion, Contemp. Math 99 (1989) 213–232.
[6] F. Merle, P. Raphael, On universality of blow-up profile for l2 critical nonlinear schrödinger equation, Invent. Math. 156 (3) (2004) 565–672.
[7] K. Moll, A. Gaeta, G. Fibich, Self-similar optical wave collapse: observation of the townes profile, Phys. Rev. Lett. 90 (20) (2003) 203902.
[8] C. Budd, S. Chen, R. Russell, New self-similar solutions of the nonlinear Schrödinger equation with moving mesh computations, J. Comput. Phys. 152 (2) (1999) 756–789.
[9] C. Budd, Asymptotics of multibump blow-up self-similar solutions of the nonlinear Schrödinger equation, SIAM J. Appl. Math. (2001) 801–830.
[10] V. Rottschäfer, T.J. Kaper, Geometric theory for multi-bump, self-similar, blowup solutions of the cubic nonlinear Schrödinger equation, Nonlinearity 16 (2003) 929–961.
[11] G. Fibich, N. Gavish, X. Wang, New singular solutions of the nonlinear Schrödinger equation, Physica D 211 (3–4) (2005) 193–220.
[12] K. McLeod, J. Serrin, Uniqueness of solutions of semilinear Poisson equations, Proc. Natl. Acad. Sci. 78 (11) (1981) 6592.
[13] N. Kopell, M. Landman, Spatial structure of the focusing singularity of the nonlinear Schroödinger equation: a geometrical analysis, SIAM J. Appl. Math. 55 (5) (1995) 1297–1323.
[14] V. Rottschäfer, T.J. Kaper, Blowup in the nonlinear Schrödinger equation near critical dimension, J. Math. Anal. Appl. 268 (2) (2002) 517–549.
[15] R. Johnson, X. Pan, On an elliptic equation related to the blow-up phenomenon in the nonlinear Schrödinger equation, Proc. Roy. Soc. Edinburgh Sect. A 123 (4) (1993) 763–782.
[16] G. Fibich, B. Ilan, Self-focusing of circularly polarized beams, Phys. Rev. E 67 (3) (2003) 036622.
[17] D. Close, C. Giuliano, R. Hellwarth, L. Hess, F. McClung, W. Wagner, The self-focusing of light of different polarizations, IEEE J. Quantum Electron. QE-2 (1966) 553–557.
[18] G. Fibich, N. Gavish, Theory of singular vortex solutions of the nonlinear Schrödinger equation, Physica D 237 (21) (2008) 2696–2730.
[19] F. Shi, Asymptotic Blowup Vortex Solutions of The Nonlinear Schrödinger Equation, (Master's thesis), Mathematisch Instituut Universiteit Leiden, The Netherlands, 2010.
[20] C. Elphick, E. Meron, E.A. Spiegel, Patterns of propagating pulses, SIAM J. Appl. Math. 50 (2) (1990) 490–503.